

<https://doi.org/10.1038/s44298-025-00126-9>

Characterization of A(H1N1)pdm09 influenza viruses isolated between 2016 and 2019



Luthfi Muawan^{1,5}, Kosuke Takada^{1,5}, Sara Yoshimoto¹, Yurie Kida¹, Shinji Watanabe² & Tokiko Watanabe^{1,3,4}

The A(H1N1)pdm09 virus, which caused the 2009 influenza pandemic, has continued to circulate in humans for over a decade. Understanding its biological properties is crucial for effective surveillance, prevention, and control. Here, we characterized recently circulating A(H1N1)pdm09 viruses, focusing on strains isolated between 2016 and 2019. HA gene-based phylogenetic tree analysis revealed that post-pandemic A(H1N1)pdm09 virus strains circulating between 2016 and 2019 form two clusters: subclade 6B.1 and subclade 6B.1 A.5a. Growth kinetics of nine selected representative strains from these clusters showed that subclade 6B.1 viruses replicated well in human lung cells, whereas some subclade 6B.1 A.5a viruses replicated poorly. In vivo, all viruses from both subclades caused significantly less weight loss in infected mice compared to the prototypic pandemic strain A/California/04/2009 (Cal04/2009). Additionally, virus titers in the lungs of mice infected with most viruses from subclade 6B.1 or 6B.1 A.5a were significantly lower than those in mice infected with Cal04/2009. Furthermore, evolutionary analysis suggested multiple transitions to a less pathogenic phenotype, indicating an evolutionary trend towards attenuation. These results demonstrate that A(H1N1)pdm09 viruses isolated between 2016 and 2019 are attenuated in mice, although the mutations responsible for this attenuation require further investigation. Our findings emphasize the need for continued monitoring of A(H1N1)pdm09 viruses to understand their evolutionary dynamics and potential impact on public health.

Influenza virus is a highly contagious respiratory pathogen that causes seasonal influenza outbreaks annually and occasionally triggers pandemics¹. Over the 20th and 21st centuries, this virus has caused four pandemics, including the devastating 1918 “Spanish flu”, the 1957 and 1968 pandemics, and the 2009 H1N1 pandemic². The emergence of a novel swine-origin H1N1 influenza A virus, later designated A(H1N1)pdm09, caused the first influenza pandemic of the 21st century³. This virus spread rapidly worldwide, resulting in significant morbidity and mortality, particularly among at-risk populations such as pregnant women, the elderly, and individuals with preexisting health issues^{3,4}. While public health interventions, including vaccination, successfully controlled the immediate spread of the virus, A(H1N1)pdm09 has continued to circulate as a seasonal virus^{5–7}. Consequently,

understanding the pathogenicity and evolution of the virus over this extended post-pandemic period is of value.

The influenza A(H1N1)pdm09 virus has now been circulating for more than 10 years. By 2014, it had acquired several mutations in hemagglutinin (HA); however, these mutations did not change the antigenic properties of the virus⁸. During the 2015–2016 influenza season, the A(H1N1)pdm09 virus classified as clade 6B.1 emerged, and its antigenicity changed⁹. Moreover, vaccine strains of A(H1N1)pdm09 influenza virus have been changed five times since the 2017–2018 influenza season, in response to changes in the viral antigens (<https://www.who.int/teams/global-influenza-programme/vaccines/who-recommendations/candidate-vaccine-viruses>). Studies have largely focused on the genetic drift and antigenic changes in A(H1N1)pdm09 virus, with some studies examining

¹Department of Molecular Virology, Research Institute for Microbial Diseases, The University of Osaka, Suita, Osaka, Japan. ²Research Center for Influenza and Respiratory Viruses, National Institute of Infectious Diseases, Musashimurayama, Tokyo, Japan. ³Center for Infectious Disease Education and Research, The University of Osaka, Suita, Osaka, Japan. ⁴Center for Advanced Modalities and DDS, The University of Osaka, Suita, Osaka, Japan. ⁵These authors contributed equally: Luthfi Muawan, Kosuke Takada. ✉ e-mail: tokikow@biken.osaka-u.ac.jp

changes in the pathogenicity of strains isolated between 2009 and 2017^{9–12}. However, the long-term pathogenicity of post-pandemic A(H1N1)pdm09 and how its pathogenic mechanisms have evolved over this extended timeframe remain underexplored.

Here, we characterized A(H1N1)pdm09 viruses throughout their continued circulation in humans, focusing on strains isolated between 2016 and 2019, by employing a combination of phylogenetic analysis, growth kinetics in human lung cells, and animal model experimentation to assess the virus's evolutionary and pathogenic changes.

Results

Phylogenetic analysis of A(H1N1)pdm09 isolates

To reveal the genetic diversity of A(H1N1)pdm09 viruses isolated during the pandemic and viruses isolated in the post-pandemic era, we examined the phylogenetic relationship of 46 representative virus strains isolated between 2009 (pandemic) and 2019. Isolate selection for the phylogenetic tree construction was based on previous studies that reported the genetic diversity of A(H1N1)pdm09 isolates from 2009 to 2019^{9,12} as well as vaccine strains from each season on the Northern and Southern Hemisphere seasonal influenza vaccine strain lists (<https://www.who.int/teams/global-influenza-programme/vaccines/who-recommendations/candidate-vaccine-viruses>).

The phylogenetic analysis of the HA gene revealed six clusters among the selected virus isolates (Fig. 1). The viruses isolated between 2016 and

2019 belonged to 2 distinct clusters: subclade 6B.1 for viruses isolated between 2016 and 2017, and subclade 6B.1 A.5a for viruses isolated between 2018 and 2019. Viruses belonging to subclade 6B.1 A.5a exhibited lower sequence identity to the Cal04/2009 strain compared to earlier viral isolates¹², particularly in the HA gene, with identity values ranging from 95.88% to 96.59% (Table 1). The heightened genetic diversity within the A(H1N1)pdm09 viral population suggests that the virus has undergone continued adaptation and evolution in the post-pandemic era.

Growth properties of A(H1N1)pdm09 viruses in a human lung cell line

To characterize A(H1N1)pdm09 viruses isolated between 2016 and 2019, nine representative viruses were selected from subclade 6B.1 and subclade 6B.1 A.5a based on their HA phylogenetic positions (shown in red in Fig. 1), genetic diversity, and availability of virus isolates. Among them, A/Hawaii/70/2019 is closely related to the 2019–2020 Northern Hemisphere vaccine strain A/Nebraska/14/2019, and A/Kobe/821/2017 is closely related to A/Scotland/P2/2015, the WHO-recommended vaccine strain for the 2015–2016 season. Cal04/2009 was used as a control. To assess the replicative properties of these viruses in a human lung cell line, a growth kinetics assay was performed using adenocarcinoma human alveolar basal epithelial (A549) cells. In A549 cells, subclade 6B.1 viruses did not show significantly different titers at 48 h post-infection (hpi) compared with Cal04/2009 ($5.7 \pm 0.8 \log_{10}$ plaque-

Fig. 1 | Phylogenetic tree based on the A(H1N1)pdm09 HA nucleic acid sequence. The tree was constructed by using the neighbor-joining method. Viral clades are indicated by brackets. The isolates used in this study are indicated in red. Numbers in the internal nodes indicate bootstrap values.

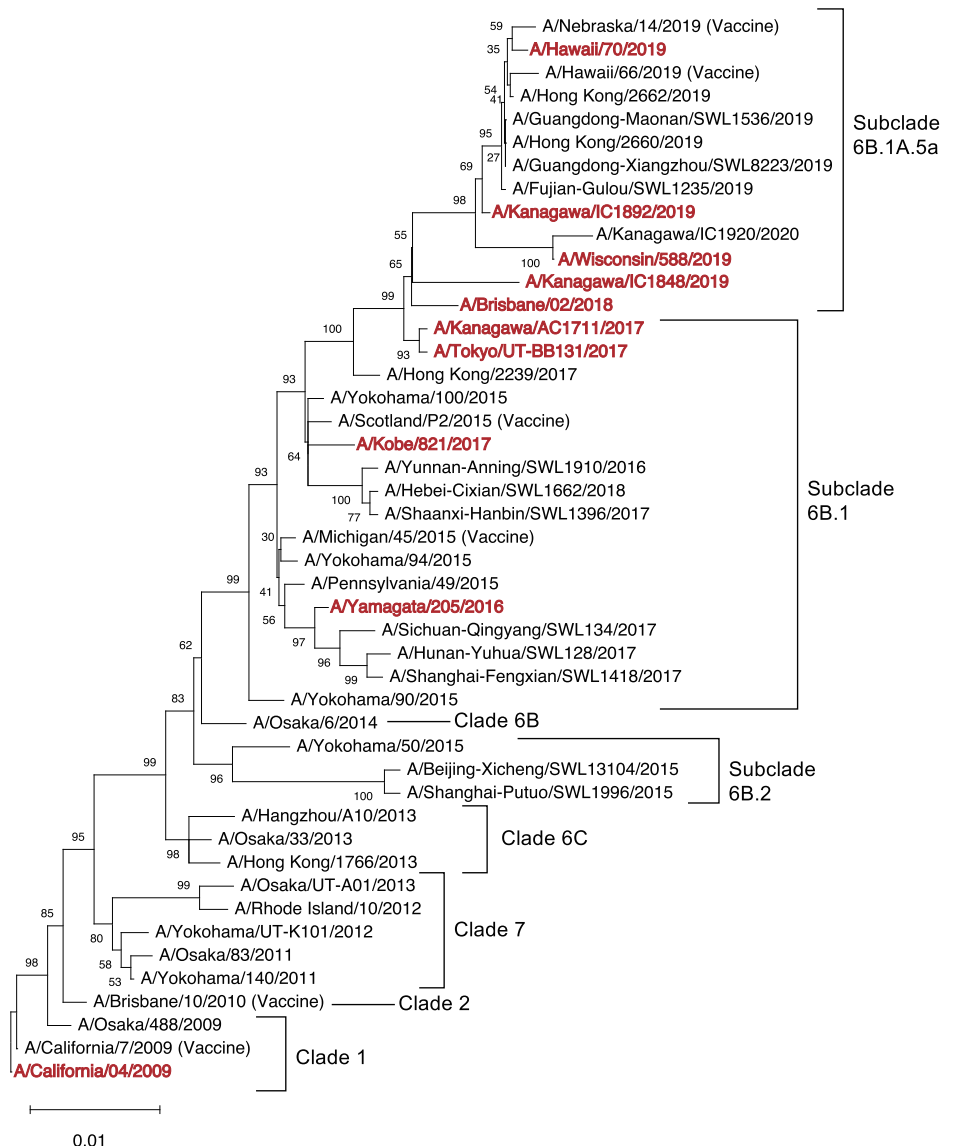
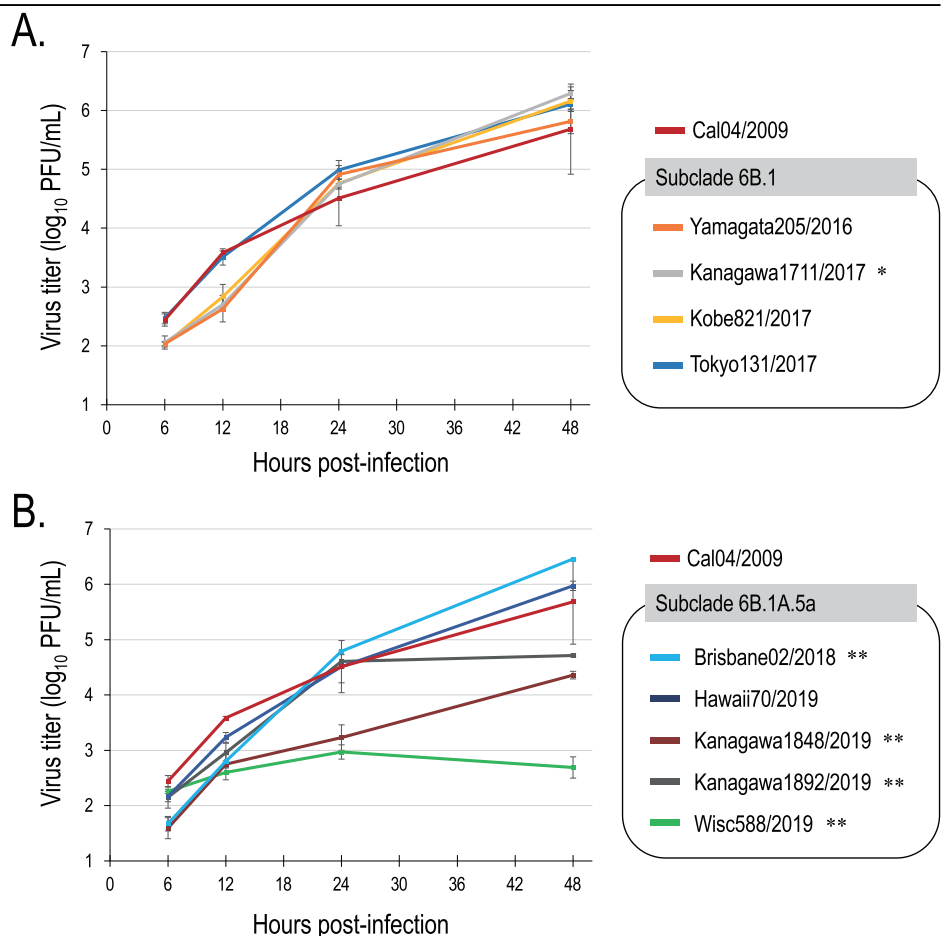


Table 1 | Sequence identity among the coding regions of the IAV genome segments compared with those of Cal04/2009

Virus	Clade	Nucleotide identity with Cal04/2009 (%) [*]							
		PB2	PB1	PA	HA	NP	NA	M	NS
A/Wisconsin/588/2019	6B.1 A.5a	97.19	97.71	97.39	95.88	97.46	96.59	97.75	96.53
A/Kanagawa/IC1892/2019		97.41	97.53	97.67	96.41	97.52	96.87	97.86	96.89
A/Kanagawa/IC1848/2019		97.50	97.93	97.53	96.06	97.46	97.09	98.47	96.42
A/Hawaii/70/2019		97.32	97.66	97.44	96.11	97.39	96.45	97.75	96.77
A/Brisbane/02/2018		97.67	98.10	97.72	96.59	97.59	97.37	98.06	97.13
A/Tokyo/UT-BB131/2017	6.B.1	97.63	98.10	97.81	96.82	97.52	97.37	98.47	97.01
A/Kobe/821/2017		97.98	98.19	98.04	97.17	97.99	97.65	98.37	97.01
A/Kanagawa/AC1711/2017		97.67	97.88	97.81	96.76	97.86	97.44	98.37	97.13
A/Yamagata/205/2016		97.80	97.97	98.09	97.41	98.06	97.80	98.67	97.25

^{*} The lowest nucleotide identities with Cal04/2009 are shown in bold.

Fig. 2 | Growth kinetics of A(H1N1)pdm09 viruses in A549 cells. (A, B) Growth kinetics of A(H1N1)pdm09 viruses in A549 cells for subclade 6B.1 (A) and subclade 6B.1 A.5a (B). Cells were infected with each A(H1N1)pdm09 virus at an MOI of 0.01. At the indicated times after infection, virus titers in the supernatant were quantified by using plaque assays. Values represent means \pm standard deviations (SD) from three independent experiments. Asterisks indicate that the virus titers were significantly higher or lower compared with Cal04/2009 at 48 hpi (*, $P < 0.05$; **, $P < 0.01$). The full results of the statistical analysis are available in the Supplementary Table S2.



forming units per milliliter [PFU/ml]), although A/Kanagawa/AC1711/2017 (Kanagawa1711/2017) showed a slightly higher titer ($P < 0.05$; $6.3 \pm 0.1 \log_{10}$ PFU/ml) (Fig. 2A). These results indicate that virus strains from subclade 6B.1 have comparable replicative ability to that of Cal04/2009 in human lung cells. In contrast, three of five viruses from subclade 6B.1 A.5a replicated less efficiently and showed 1–3 log lower titers at 48 hpi than that of Cal04/2009 ($P < 0.01$), whereas A/Hawaii/70/2019 (Hawaii70/2019) and A/Brisbane/02/2018 (Brisbane02/2018) showed similar ($5.9 \pm 0.1 \log_{10}$ PFU/ml) and higher titers ($6.5 \pm 0.2 \log_{10}$ PFU/ml; $P < 0.01$), respectively, compared to Cal04/2009 (Fig. 2B). These results suggest that subclade 6B.1 viruses replicate well in human lung cells, whereas some viruses of subclade 6B.1 A.5a replicate poorly.

Pathogenicity of A(H1N1)pdm09 viruses in a mouse model

To examine the pathogenicity of A(H1N1)pdm09 viruses isolated between 2016 and 2019 in vivo, we infected BALB/c mice intranasally with 10^5 PFU of each of nine representative strains and monitored body weight changes for up to 14 days (Fig. 3). None of the strains tested were fatal to mice. Mice infected with Cal04/2009 experienced appreciable body weight loss until day 7 post-infection with a maximum body weight loss of $11.4 \pm 3.17\%$, followed by recovery (Fig. 3 and Table 2), which is consistent with previous findings^{12,13}. In contrast, the maximum body weight loss induced by the A(H1N1)pdm09 isolates ranged from 0.8% to 5.1%, significantly lower than the body weight loss of mice infected with Cal04/2009 ($11.4 \pm 3.17\%$; $P < 0.05$) (Table 2). These results suggest that the A(H1N1)pdm09 viruses

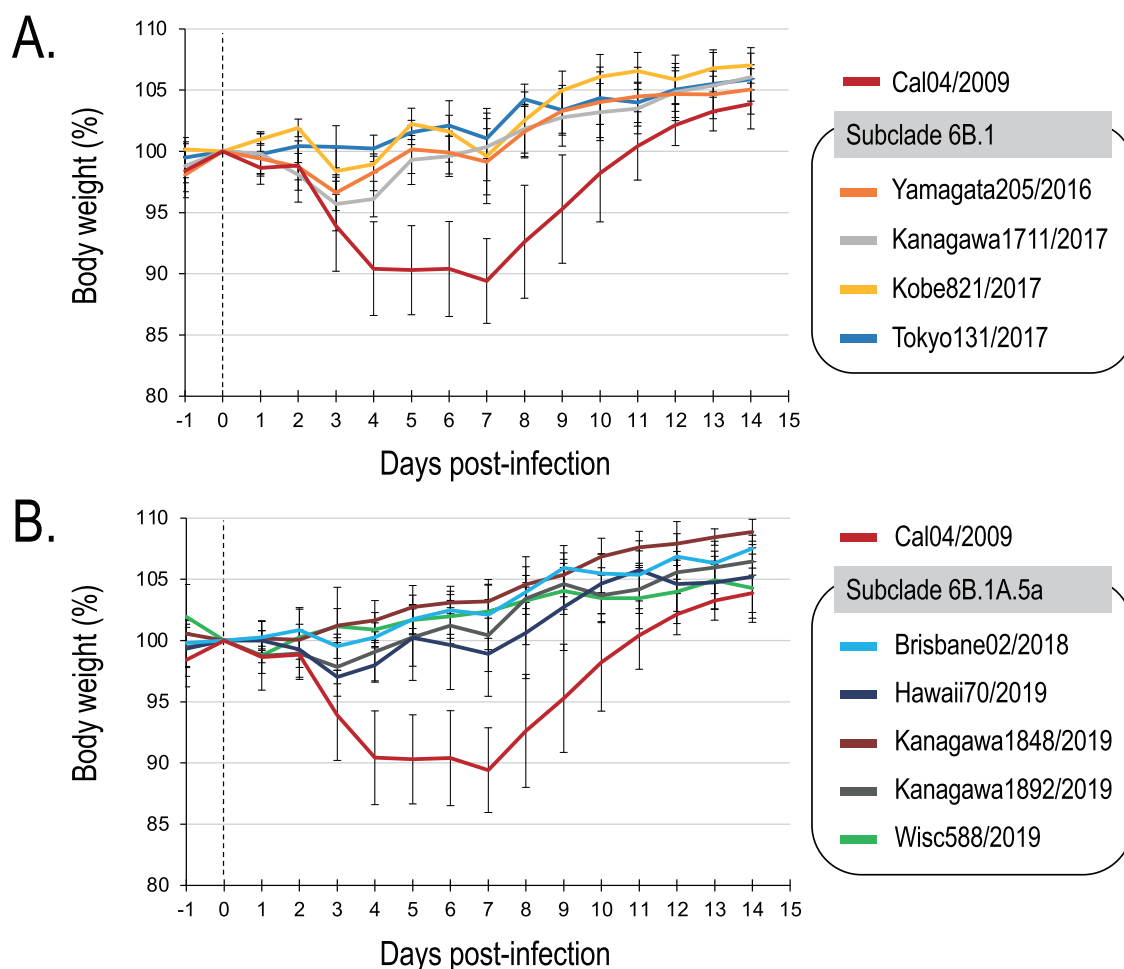


Fig. 3 | Body weight changes in mice infected with A(H1N1)pdm09 viruses. (A, B) Body weight changes in mice infected with viruses from subclade 6B.1 (A) and subclade 6B.1 A.5a (B). Five mice per group were intranasally inoculated with 10^5

PFU (in 50 μ l) of the virus strains. Body weights were monitored daily for 14 days. The values represent average scores of overall body weight loss compared with initial body weight \pm SD from five mice (or four mice for Cal04/2009).

Table 2 | Pathogenicity of A(H1N1)pdm09 viruses

Virus	% of mean maximum body weight loss ^a (Mean \pm SD)	Clade
A/Wisconsin/588/2019	2.0 \pm 2.17*	6B.1 A.5a
A/Kanagawa/IC1892/2019	2.8 \pm 1.63*	6B.1 A.5a
A/Kanagawa/IC1848/2019	0.8 \pm 0.50*	6B.1 A.5a
A/Hawaii/70/2019	3.5 \pm 1.58*	6B.1 A.5a
A/Brisbane/02/2018	0.9 \pm 0.80*	6B.1 A.5a
A/Tokyo/UT-BB131/2017	1.0 \pm 0.95*	6B.1
A/Kobe/821/2017	2.6 \pm 1.94*	6B.1
A/Kanagawa/AC1711/2017	5.1 \pm 1.42*	6B.1
A/Yamagata/205/2016	3.4 \pm 1.46*	6B.1
A/California/04/2009	11.4 \pm 3.17	1

^a The percentage of maximum body weight loss was calculated by comparing the greatest decrease in body weight for each infected mouse to its initial body weight.

*Asterisks indicate significant body weight changes compared to Cal04/2009 ($P < 0.05$). The full results of the statistical analysis are available in the Supplementary Table S3.

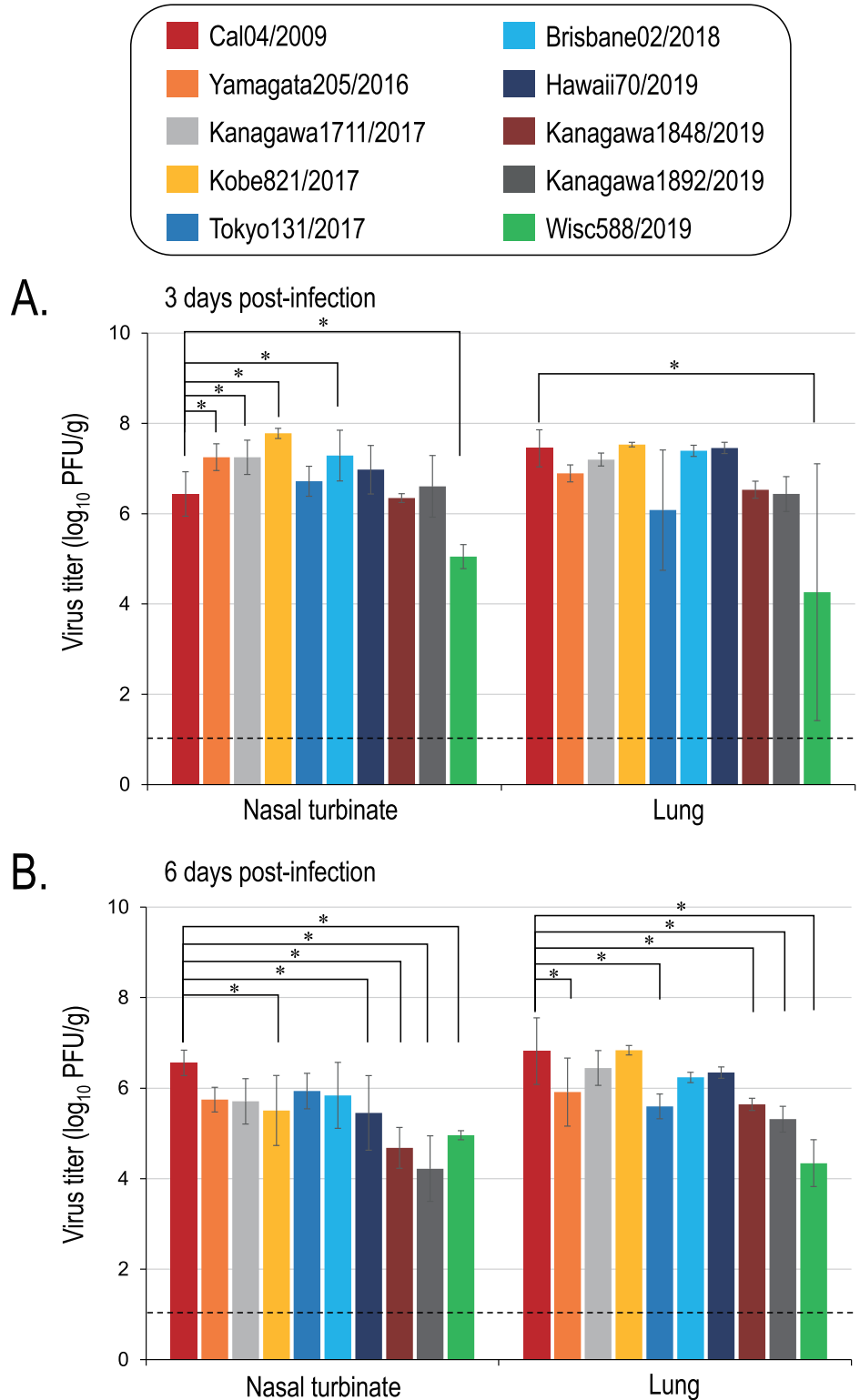
isolated between 2016 and 2019 are less pathogenic to mice than Cal04/2009.

Replicative ability of A(H1N1)pdm09 viruses in mice

Next, to assess the replicative ability of A(H1N1)pdm09 viruses in mouse respiratory organs, mice were infected with 10^5 PFU of virus, and organ titers were determined. At 3 days post-infection (dpi), all viruses were detected in the nasal turbinate, and subclade 6B.1 viruses, except for A/Tokyo/UT-BB131/2017 (Tokyo131/2017), showed significantly higher titers compared to those of Cal04/2009 at 3 dpi (7.2 ± 0.4 to 7.8 ± 0.1 log₁₀ PFU/g; $P < 0.05$) (Fig. 4). Brisbane02/2018 and Hawaii70/2019 in subclade 6B.1 A.5a replicated more efficiently than Cal04/2009, whereas A/Kanagawa/IC1892/2019 (Kanagawa1892/2019) and A/Kanagawa/IC1848/2019 (Kanagawa1848/2019) were comparable, and A/Wisconsin/588/2019 (Wisc588/2019) titers were significantly lower than those of Cal04/2009. These results indicate that virus strains in subclade 6B.1 have the same or higher replicative ability compared to that of Cal04/2009 in mouse nasal turbinate, but some viruses in subclade 6B.1 A.5a have lower replicative ability than Cal04/2009. In the lung, all viruses were detected at 3 dpi, except for one mouse infected with Wisc588/2019. Wisc588/2019, in subclade 6B.1 A.5a, replicated significantly less efficiently than Cal04/2009, exhibiting 4.3 ± 2.8 log₁₀ PFU/g in lung at 3 dpi ($P < 0.05$). At 6 dpi, all viruses were detected in the nasal turbinate and lung. The mean titer in the nasal

Fig. 4 | A(H1N1)pdm09 virus titers in the respiratory organs of infected mice. (A, B)

A(H1N1)pdm09 virus titers in the respiratory organs of infected mice (four mice per group) at 3 (A) and 6 (B) dpi. Each viral strain was intranasally administered to mice at a dose of 10^5 PFU. At 3 and 6 dpi, organs from the mice were collected, and a plaque assay was used to quantify the virus titer. Asterisks indicate statistically significant differences in viral titers compared to Cal04/2009 ($P < 0.05$). The full results of the statistical analysis are available in the Supplementary Table S4. The limit of detection (LOD) for the plaque test is shown by the dashed black line at the concentration of 1×10^1 PFU/g.



turbinate of mice infected with subclade 6B.1 viruses was slightly lower than that of Cal04/2009, whereas four of five viruses in subclade 6B.1 A.5a showed significantly lower titers than that of Cal04/2009 (4.2 ± 0.7 to 5.5 ± 0.8 \log_{10} PFU/g; $P < 0.05$). In the lung, the titers of three of five viruses in subclade 6B.1 A.5a and two of four viruses in subclade 6B.1 were also significantly lower than that of Cal04/2009 (Fig. 4). These results suggest that the viruses of subclades 6B.1 and 6B.1 A.5a tend to replicate less well in mouse lung than Cal04/2009, and that some viruses in subclade 6B.1

replicate more efficiently in the mouse nasal turbinate than Cal04/2009. Some subclade 6B.1 A.5a viruses replicate less efficiently in the mouse nasal turbinate than Cal04/2009.

Estimation of evolutionary patterns of pathogenicity in A(H1N1)pdm09 gene segments

To gain a more comprehensive understanding of the possible evolutionary trajectories of A(H1N1)pdm09 pathogenicity, we analyzed the evolutionary

A.

Gene segment	Number of transitions	Parsimonious patterns
PB2	4	1
PB1	5	1
PA	4	1
HA	5	4
NP	4	1
NA	5	1
M	5	2
NS	5	1

B.

 Transition to be less pathogenic

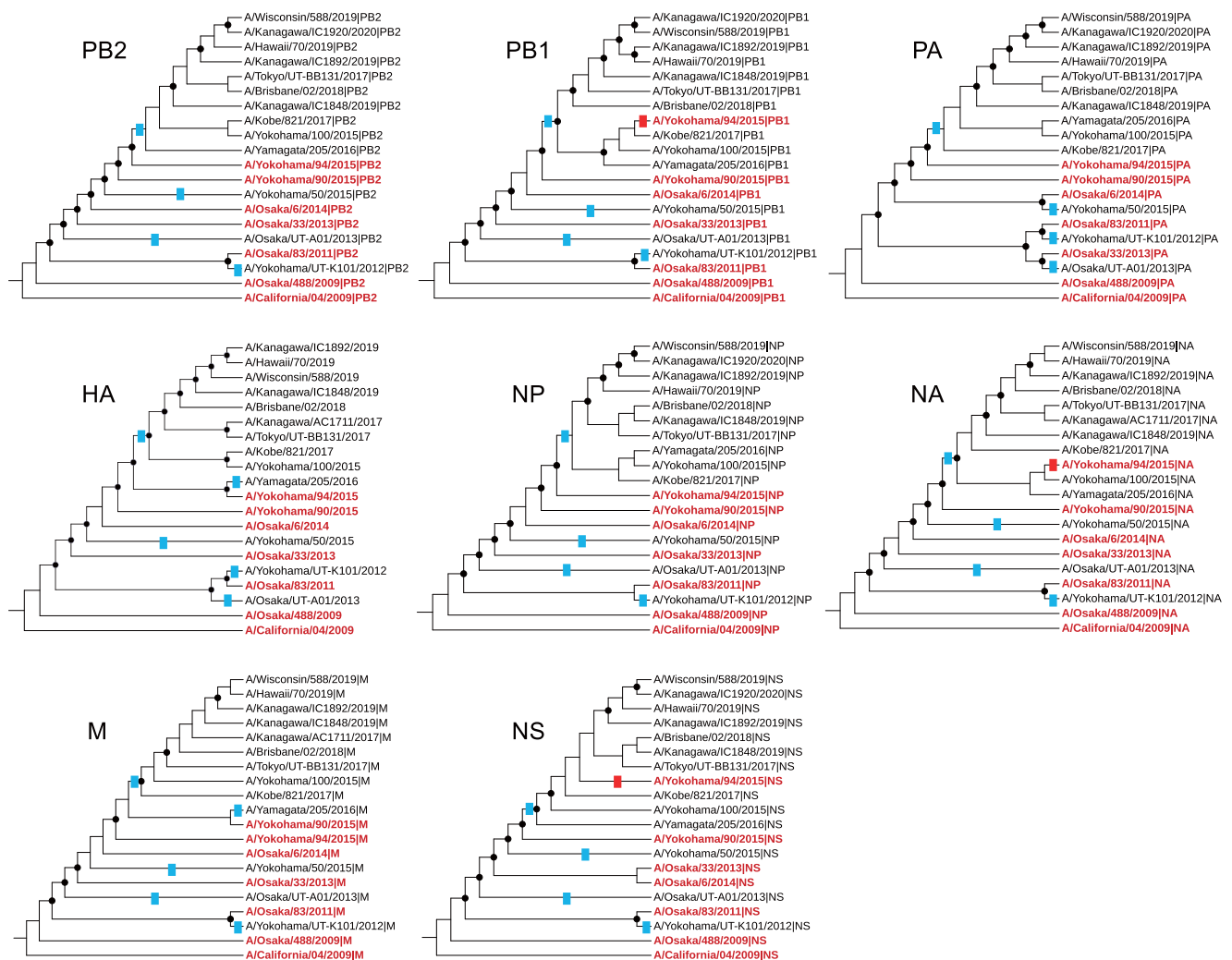
 Reversion to be pathogenic


Fig. 5 | Estimation of the most likely transition patterns based on the parsimonious patterns of pathogenicity transition of representative A(H1N1)pdm09 strains from 2009 to 2019. A Estimation of the number and patterns of pathogenicity transitions under the minimum-transition scenario. **B** Visualization of pathogenicity transitions on the phylogenetic tree, based on the most likely transition patterns. The blue and red lines indicate transitions to be less pathogenic and reversion to be pathogenic, respectively. The phylogenetic tree was constructed

based on strains from this study, with the addition of strains from previous studies¹². A black circle in an internal node corresponds to bootstrap values $\geq 70\%$. The red color denotes strains with high pathogenicity, whereas the black color denotes strains with low pathogenicity. Pathogenicity was determined based on the body weight loss of mice infected with the respective virus, with strains that caused significantly less body weight loss compared with Cal04/2009 being considered to have low pathogenicity.

transition patterns with respect to the pathogenicity of the virus strains from this study, coupled with data from prior similar studies of the same viral strains¹². We estimated parsimonious patterns, where pathogenicity transitions occurred a minimum number of times (Fig. 5A and Supplementary Fig. S1) and then selected the most likely patterns (Fig. 5B). Our analysis estimated that the minimum number of transitions was four for PB2, PA, and NP and five for PB1, HA, NA, M, and NS (Fig. 5A). Among the gene segments, PB1, PB2, PA, NP, NA, and NS showed only one parsimonious pattern, whereas HA and M exhibited greater diversity, with four and two transition patterns, respectively (Fig. 5A and Supplementary Fig. S1). The evolutionary trajectories suggested multiple transitions toward reduced pathogenicity in several genes (Figs. 5A, B, and Supplementary Fig. S1). Interestingly, reversions to pathogenic viruses were observed in the PB1, HA, NA, M, and NS genes, although these reversions did not result in the establishment of stable pathogenic clusters (Fig. 5B and Supplementary Fig. S1). These data suggest that the viral population continues to evolve in a predominantly attenuating direction, even when transient reversions to higher pathogenicity occur. Overall, our findings indicate that A(H1N1)pdm09 has undergone evolutionary changes that favor reduced pathogenicity over time.

Discussion

Here we characterized A(H1N1)pdm09 virus isolates from 2016 to 2019, which belonged to subclades 6B.1 and 6B.1 A.5a based on our phylogenetic analysis of their HA genes. In previous studies, early A(H1N1)pdm09 isolates such as A/California/07/2009 (which belongs to the original pandemic clade) and A/Bolivia/559/2013 (clade 6B.1) replicated well in A549 cells, albeit with reduced multi-cycle infectivity compared to pre-2009 H1N1 strains¹⁴. Furthermore, clade 6B.1 viruses, such as A/Guangdong/887/2017 and A/Guangdong/752/2017, were found to replicate efficiently in A549 cells⁹. Consistent with these previous findings, we found that the subclade 6B.1 viruses in our study replicated well in A549 cells (Fig. 2A). Some studies have reported that certain mutations can enhance influenza virus replication in A549 cells. For instance, some A(H1N1)pdm09 strains with V100I, P224S, N321K, I330V, and R362K substitutions in their PA proteins and E55K, L90I, I123V, E125D, K131E, N205S in their NS1 proteins (circulating during the 2015–2016 and 2016–2017 seasons) showed higher replication titers than the early pandemic strain Cal04/2009 (clade 1) in A549 cells^{9,11}. However, our results showed reduced replicative efficiency of more recent strains in A549 cells despite having the same amino acid substitutions in their PA and NS1 proteins, except for Kanagawa1848/2019, which has N205R rather than N205S in its NS1 protein. Some strains from subclade 6B.1 A.5a replicated poorly, especially Wisc588/2019, which showed viral titers 3 logs lower than that of Cal04/09 (Fig. 2B). Similarly, Wisc588/2019 replicated poorly in humanized Madin-Darby canine kidney (hCK) cells (see Supplementary information and Supplementary Fig. S2)¹⁵. These findings suggest that there are other factors that may affect A(H1N1)pdm09 viral replication efficiency in human lung cells that should be investigated further.

Our data also demonstrate that isolates from 2016 to 2019 show decreased pathogenicity and replicative ability compared to Cal04/2009 in a mouse model. Wisc588/2019, in particular, exhibited the lowest viral titers in mouse lungs (Figs. 3 and 4, and Table 2), leading to attenuation in mice. In contrast, A/Kanagawa/AC1711/2017 replicated efficiently in both human lung cells and the lungs of infected mice, yet showed lower pathogenicity than Cal04/2009. These findings suggest that factors beyond viral replication—such as host immune responses or virus–host interactions—may contribute to attenuated disease outcomes. In this context, several amino acid differences were identified in the viral proteins of Cal04/2009 compared to those of recent attenuated strains (Supplementary Table S5); the functional relevance of these substitutions remains to be elucidated. In a previous study, some Japanese A(H1N1)pdm09 isolates from 2009 to 2015 showed a range of pathogenicity in mice, from milder to more severe than that of Cal04/2009¹². Our findings contradict a previous finding that some A(H1N1)pdm09 virus strains circulating during the 2015–2016 season

acquired amino acid changes (i.e., V100I, N204S, R221Q, and L229S) in PA-X proteins that enhanced their ability to suppress host gene expression, potentially increasing virus replication, and leading to higher replicative ability in A549 cells and higher pathogenicity in mice, compared to the original pandemic strain¹¹. All nine influenza strains in this study shared those same amino acid substitutions in their PA-X protein despite showing reduced pathogenicity in mice. This difference suggests that the recent strains may have acquired other genetic mutations that may be involved in reduced pathogenicity. Given that multiple genes and mutations affect the pathogenicity of influenza viruses^{9,11,16}, it is possible that several genes and mutations may also be affected in A(H1N1)pdm09. Further investigation is needed to understand the attenuation of recently circulating A(H1N1)pdm09 viruses in this human lung cell line and in a mouse model.

The pathogenicity of RNA viruses can change over time. We estimated the pathogenicity evolutionary patterns of our representative A(H1N1)pdm09 viruses isolated between 2016 and 2019 and found that these viruses appear to have become less pathogenic with the passage of time. While occasional reversions to a more pathogenic phenotype were identified, our analysis suggests that these reverted strains are unlikely to diversify or sustain widespread circulation (Fig. 5B and Supplementary Fig. S1). One limitation of this study is that we evaluated only a subset of representative viral strains, which may not comprehensively reflect the evolutionary trajectories of the entire A(H1N1)pdm09 population. Further studies using a broader and more diverse selection of virus strains may be helpful. Nonetheless, a previous study speculated that more pathogenic phenotypes are likely outcompeted by variants exhibiting greater fitness for transmission and host adaptation¹⁷. Even for the recent coronavirus pandemic virus, SARS-CoV-2, experiments with animal models have shown that the Omicron strain, which emerged in late 2021, has significantly reduced pathogenicity compared to the original Wuhan strain that emerged in China in 2019^{18–21}. These trends may be because slightly deleterious mutations accumulate based on the nearly neutral theory of molecular evolution^{22,23}. The observed decrease in pathogenicity over time may represent a broader evolutionary pattern among pandemic viruses, not unique to the A(H1N1)pdm09 influenza virus. Our findings enhance our understanding of the evolution, replication, and pathogenicity of the A(H1N1)pdm09 influenza virus. As this virus continues to evolve, it is essential to sustain comprehensive surveillance efforts to help control the further spread of the A(H1N1)pdm09 strain.

Methods

Cells

Madin-Darby canine kidney (MDCK) cells were grown in minimal essential medium (MEM) with 5% newborn calf serum and 1% penicillin–streptomycin (PS). hCK cells²⁴ were grown in minimal essential medium (MEM) with 5% newborn calf serum, 1% PS, 10 µg/mL blasticidin, and 2 µg/mL puromycin. A549 cells were grown in F-12K Medium (Kaighn's Modification of Ham's F-12 Medium) with Fetal Bovine Serum (FBS) and 1% PS. Cells were maintained at 37 °C in 5% CO₂. MDCK and hCK cells were used for plaque assays. A549 and hCK cells were used for growth kinetics assays.

Viruses

In this study, we used the following A(H1N1)pdm09 viruses: A/Wisconsin/588/2019 (Wisc588/2019), A/Kanagawa/IC1848/2019 (Kanagawa1848/2019), A/Hawaii/70/2019 (Hawaii70/2019), A/Kanagawa/IC1892/2019 (Kanagawa1892/2019), A/Brisbane/02/2018 (Brisbane02/2018), A/Kanagawa/AC1711/2017 (Kanagawa1711/2017), A/Kobe/821/2017 (Kobe821/2017), A/Tokyo/UT-BB131/2017 (Tokyo131/2017), and A/Yamagata/205/2016 (Yamagata205/2016). In addition, we used A/California/04/2009 (Cal04/2009), which is the prototypic pandemic strain, as a reference strain since we used this strain in our previous study¹². Cal04/2009 was grown in MDCK cells at 37 °C to make stock viruses; the other strains were grown in hCK cells at 33 °C. Cal04/2009 was generated by reverse genetics as previously described¹³. Tokyo131/2017 was kindly provided by Professor

Yoshihiro Kawaoka (The University of Tokyo). The other strains were clinical isolates obtained from the National Institute of Infectious Diseases (NIID, Japan).

Sequencing

Briefly, viral RNA was isolated from the supernatants of virus-infected MDCK or hCK cells by using a QIAamp viral RNA minikit (Qiagen, Hilden, Germany). The extracted RNA was subjected to reverse transcription using M-MLV Reverse Transcriptase (Invitrogen, Waltham, MA, USA) and the Uni12 universal primers 24, which are designed specifically for the genes of influenza A virus, to generate cDNA. To amplify each A(H1N1)pdm09 virus gene from the synthesized cDNA, the resulting products were PCR-amplified using PrimeSTAR Max DNA Polymerase (Takara Bio, San Jose, CA, USA) and Hoffmann universal primers specific for the eight influenza A viral RNA segments²⁵. The PCR products were purified using the Gel/PCR DNA Isolation System (Viogene, New Taipei, Taiwan). The purified products were sequenced using the Sanger Sequencing method. The sequences were assembled and analyzed using GENETYX-MAC software (version 22.0.1, Tokyo, Japan).

Phylogenetic analysis

For our phylogenetic analysis, we selected 46 A(H1N1)pdm09 strains isolated between 2009 and 2019. The selection was based on: (1) geographical and temporal diversity; (2) previously reported genetic variation^{9,12}; and (3) inclusion of WHO-recommended vaccine strains for each season in the Northern and Southern Hemispheres. The phylogenetic tree was constructed using nucleic acid sequences from the HA gene of A(H1N1)pdm09 viruses (Supplementary Table S1) with the neighbor-joining method²⁶ using Kimura distances²⁷ and the 1000 replicates bootstrap using Molecular Evolutionary Genetics Analysis (MEGA) software (version 11.0.13, Pennsylvania, USA). Nucleic acid sequences from seven other segments (PB1, PB2, PA, NA, NP, M, and NS) were used to construct supporting phylogenetic trees (Supplementary Fig. S3). All sequences were aligned by using the MUSCLE (Multiple Sequence Comparison by Log-Expectation) algorithm²⁸. The Cal04/2009 sequence was used to root each tree. The nucleic acid sequences of the A(H1N1)pdm09 isolates were retrieved from the EpiFlu database (<https://www.gisaid.org/>), and the HA genetic clades were identified by using representative isolates from each clade available through the EpiFlu database.

Growth kinetics assay

Duplicate wells of confluent A549 and hCK cells were infected with viruses at a multiplicity of infection (MOI) of 0.01 with MEM containing 0.3% bovine serum albumin (BSA) and 1 µg/mL tosylsulfonfyl phenylalanyl chloromethyl ketone (TPCK)-treated trypsin and incubated at 37 °C in 5% CO₂. Supernatants were harvested at 6, 12, 24, and 48 hpi. Virus titers were determined by performing plaque assays with MDCK or hCK cells. Each assay was run in duplicate wells and performed in three independent experiments.

Mouse experiments

All animal experiments were approved by the Animal Research Committee of the Research Institute for Microbial Diseases, the University of Osaka. All animals were maintained in pathogen-free conditions in a temperature and humidity-controlled environment with a 12 h:12 h light-dark cycle and *ad libitum* access to water and standard laboratory food. Virus inoculations were conducted under anesthesia using isoflurane, and every attempt was made to reduce animal suffering.

Six-week-old female BALB/c mice weighing 15–20 g (Japan SLC, Inc., Shizuoka, Japan) were used in this study to be consistent with a previous study¹². Baseline body weights were measured prior to infection. Five or four mice per group were anesthetized with isoflurane and then intranasally inoculated with 10⁵ PFU in 50 µL of virus in phosphate-buffered saline (PBS). Body weight and survival were monitored daily for 14 dpi. The percentage of body weight change was calculated by comparing the weight of each mouse at each time point to its initial weight on day 0. The

percentage of maximum body weight loss was determined by comparing the minimum body weight of each mouse to its initial body weight. Mice that showed any signs of severe disease or experienced weight loss of more than 30% of their initial body weight were euthanized.

To assess viral replicative ability in respiratory organs, eight mice per group were infected intranasally with 10⁵ PFU (in 50 µL) of viruses in PBS. At 3- and 6-dpi, four mice were euthanized, and their lungs and nasal turbinates were collected, homogenized with MEM containing 0.3% BSA, and titrated in MDCK or hCK cells by use of plaque assays.

Estimation of evolutionary patterns of pathogenicity

A phylogenetic tree of A(H1N1)pdm09 viruses was constructed by using the nucleic acid sequences of eight genes with the neighbor-joining method (Kimura distances, 1000 bootstrap replicates) in MEGA (v11.0.13). Sequences were aligned with the MUSCLE algorithm, and Cal04/2009 was used as the root. To investigate evolutionary transition patterns in the pathogenicity of the viruses, the pathogenic transition patterns were mapped onto phylogenetic trees for each gene segment by estimating of the most likely transitions based on the parsimonious patterns, branch length, and a nearly neutral theory of molecular evolution^{22,23}; pathogenicity data in mice (based on body weight loss) were correlated with the appropriate evolutionary branches. Each pathogenicity transition was identified and labelled in accordance with the parsimonious patterns of the pathogenicity transitions, which minimized the number of evolutionary changes²⁹.

Statistical analysis

To assess statistical differences across the datasets, GraphPad Prism (version 9.5.1, GraphPad Software, USA) was used. For in vitro and in vivo growth kinetics data, a two-way analysis of variance (ANOVA) and Tukey's multiple comparisons post-hoc test were used. For pathogenicity data in mice, a one-way ANOVA and Dunnett's multiple comparisons post-hoc test were used. Statistical significance was indicated when the *P*-value was less than 0.05 (*P* < 0.05).

Data availability

The data underlying this article will be shared on reasonable request to the corresponding author.

Code availability

No custom code was used during the data analysis.

Received: 27 January 2025; Accepted: 8 May 2025;

Published online: 22 May 2025

References

1. Neumann, G. et al. In *Fields Virology* (eds. Knipe, D. et al.) vol. 1, 649–705 (Lippincott Williams & Wilkins, Philadelphia, 2021).
2. Krammer, F. & Palase, P. In *Fields Virology* (eds. Howley, P. M. et al.) vol. 1, 596–648 (Lippincott Williams & Wilkins, Philadelphia, 2021).
3. Dawood, F. S. et al. Emergence of a novel Swine-origin Influenza A (H1N1) virus in humans. *N. Engl. J. Med.* **360**, 2605–2615 (2009).
4. Garten, R. J. et al. Antigenic and genetic characteristics of Swine-origin 2009 A(H1N1) Influenza viruses circulating in humans. *Science* **325**, 197–201 (2009).
5. Morens, D. M., Taubenberger, J. K. & Fauci, A. S. The 2009 H1N1 pandemic influenza virus: what next?. *mBio* **1**, e00211–10 (2010).
6. Neumann, G. & Kawaoka, Y. The first influenza pandemic of the new millennium. *Influenza Other Respir. Viruses* **5**, 157–166 (2011).
7. Su, Y. C. F. et al. Phylodynamics of H1N1/2009 influenza reveals the transition from host adaptation to immune-driven selection. *Nat. Commun.* **6**, 7952 (2015).
8. Goka, E. A., Vally, P. J., Mutton, K. J. & Klapper, P. E. Mutations associated with severity of the pandemic influenza A(H1N1)pdm09 in humans: a systematic review and meta-analysis of epidemiological evidence. *Arch. Virol.* **159**, 3167–3183 (2014).

9. Sun, H. et al. The genetic diversity, replication, and transmission of 2009 pandemic H1N1 viruses in China. *Front. Microbiol.* **14**, 1110100 (2023).
10. Soga, T. et al. Characterization of influenza A(H1N1)pdm09 viruses isolated in the 2018–2019 and 2019–2020 influenza seasons in Japan. *Viruses* **15**, 535 (2023).
11. Nogales, A., Martinez-Sobrido, L., Chiem, K., Topham, D. J. & DeDiego, M. L. Functional evolution of the 2009 pandemic H1N1 influenza virus NS1 and PA in humans. *J. Virol.* **92**, e01206–e01218 (2018).
12. Mitake, H. et al. Comparison of the pathogenicity in mice of A(H1N1)pdm09 viruses isolated between 2009 and 2015 in Japan. *Viruses* **12**, 155 (2020).
13. Uraki, R. et al. Virulence determinants of pandemic A(H1N1)2009 influenza virus in a mouse model. *J. Virol.* **87**, 2226–2233 (2013).
14. Hawksworth, A. et al. Replication of live attenuated influenza vaccine viruses in human nasal epithelial cells is associated with H1N1 vaccine effectiveness. *Vaccine* **38**, 4209–4218 (2020).
15. Takada, K., Kida, Y., Watanabe, S. & Watanabe, T. Influenza B viruses are more susceptible to high temperatures than influenza A viruses. *npj Viruses* **2**, 65 (2024).
16. Kim, W.-J., Hur, K.-Y., Park, H. W., Lee, S.-W. & Yoo, J.-Y. Pathogenicity of the H1N1 influenza virus enhanced by functional synergy between the NPV100I and NAD248N pair. *PLoS One* **14**, e0217691 (2019).
17. Lyons, D. M. & Llaure, A. S. Mutation and epistasis in influenza virus evolution. *Viruses* **10**, 407 (2018).
18. Tamura, T. et al. Virological characteristics of the SARS-CoV-2 Omicron XBB.1.5 variant. *Nat. Commun.* **15**, 1176 (2024).
19. Tamura, T. et al. Comparative pathogenicity of SARS-CoV-2 Omicron subvariants including BA.1, BA.2, and BA.5. *Commun. Biol.* **6**, 772 (2023).
20. Hattab, D., Amer, M. F. A., Al-Alami, Z. M. & Bakhtiar, A. SARS-CoV-2 journey: from alpha variant to omicron and its sub-variants. *Infection* **52**, 767–786 (2024).
21. Takada, K. et al. Genes involved in the limited spread of SARS-CoV-2 in the lower respiratory airways of hamsters may be associated with adaptive evolution. *J. Virol.* **98**, e0178423 (2024).
22. Hughes, A. L. Near neutrality. *Ann. N. Y. Acad. Sci.* **1133**, 162–179 (2008).
23. Ohta, T. Slightly deleterious mutant substitutions in evolution. *Nature* **246**, 96–98 (1973).
24. Takada, K. et al. A humanized MDCK cell line for the efficient isolation and propagation of human influenza viruses. *Nat. Microbiol.* **4**, 1268–1273 (2019).
25. Hoffmann, E., Stech, J., Guan, Y., Webster, R. G. & Perez, D. R. Universal primer set for the full-length amplification of all influenza A viruses. *Arch. Virol.* **146**, 2275–2289 (2001).
26. Saitou, N. & Nei, M. The neighbor-joining method: a new method for reconstructing phylogenetic trees. *Mol. Biol. Evol.* <https://doi.org/10.1093/oxfordjournals.molbev.a004054> (1987).
27. Kimura, M. A simple method for estimating evolutionary rates of base substitutions through comparative studies of nucleotide sequences. *J. Mol. Evol.* **16**, 111–120 (1980).
28. Edgar, R. C. MUSCLE: multiple sequence alignment with high accuracy and high throughput. *Nucleic Acids Res.* **32**, 1792–1797 (2004).
29. Fitch, W. M. Toward defining the course of evolution: minimum change for a specific tree topology. *Syst. Zool.* **20**, 406 (1971).

Acknowledgements

We thank Susan Watson for scientific editing. We also thank Mikiko Tanaka and Tomomi Kirino for excellent technical assistance, and Kanako

Hiromatsu for secretarial work. In addition, we thank Prof. Yoshihiro Kawaoka for kindly providing viruses. We gratefully acknowledge all data-contributing scientists and medical staff, their originating laboratories responsible for obtaining the specimens, and their submitting laboratories for generating the genetic sequences and metadata and sharing via the GISAID Initiative (Supplementary Table S1). This study was supported by JSPS KAKENHI Grants-in-Aid for Scientific Research (B) [JP22H02521 (to T.W.)]; a Grant-in-Aid for Early-Career Scientists [25K18814 (to K.T.)]; the AMED Research Program on Emerging and Re-emerging Infectious Diseases [JP19fk0108113 (to T.W.)]; AMED under Grant Numbers JP223fa627002, JP22am0401030, and JP23fk0108659 (to T.W.); AMED Advanced Research and Development Programs for Medical Innovation (AMED-CREST) [JP22gm1610010 (to T.W.)]; the Takeda Science Foundation (to T.W.); and RIKAKEN HOLDINGS CO. Young Researcher Support Grant-in-aid (to K.T.). The study was also supported by the Grant for Joint Research Project of the Research Institute for Microbial Diseases, the University of Osaka.

Author contributions

K.T. and T.W. conceptualized the study. L.M., K.T., and S.Y. performed the in vivo experiments. L.M., K.T., and Y.K. performed the in vitro experiments. L.M. and K.T. analyzed the genome sequence data. L.M., K.T., S.W., and T.W. wrote the manuscript. All authors read and approved the final manuscript.

Competing interests

The authors declare no competing interests.

Additional information

Supplementary information The online version contains supplementary material available at <https://doi.org/10.1038/s44298-025-00126-9>.

Correspondence and requests for materials should be addressed to Tokiko Watanabe.

Reprints and permissions information is available at <http://www.nature.com/reprints>

Publisher's note Springer Nature remains neutral with regard to jurisdictional claims in published maps and institutional affiliations.

Open Access This article is licensed under a Creative Commons Attribution-NonCommercial-NoDerivatives 4.0 International License, which permits any non-commercial use, sharing, distribution and reproduction in any medium or format, as long as you give appropriate credit to the original author(s) and the source, provide a link to the Creative Commons licence, and indicate if you modified the licensed material. You do not have permission under this licence to share adapted material derived from this article or parts of it. The images or other third party material in this article are included in the article's Creative Commons licence, unless indicated otherwise in a credit line to the material. If material is not included in the article's Creative Commons licence and your intended use is not permitted by statutory regulation or exceeds the permitted use, you will need to obtain permission directly from the copyright holder. To view a copy of this licence, visit <http://creativecommons.org/licenses/by-nc-nd/4.0/>.

© The Author(s) 2025